SCIENCE CHINA
Information Sciences

• RESEARCH PAPER •

August 2022, Vol. 65 182402:1–182402:9
https://doi.org/10.1007/s11432-021-3398-y

Efficient heterogeneous integration of InP/Si and GaSb/Si templates with ultra-smooth surfaces

Tingting JIN[1,2†], Jiajie LIN[3†*], Tiangui YOU[1], Xiaolei ZHANG[1,2,4], Hao LIANG[1,2], Yifan ZHU[1,2], Jialiang SUN[1,2], Hangning SHI[1,2], Chaodan CHI[1,2], Min ZHOU[1], Robert KUDRAWIEC[5], Shumin WANG[6*] & Xin OU[1*]

[1]*State Key Laboratory of Functional Materials for Informatics, Shanghai Institute of Microsystem and Information Technology, Chinese Academy of Sciences, Shanghai* 200050*, China;*
[2]*Center of Materials Science and Optoelectronics Engineering, University of Chinese Academy of Sciences, Beijing* 100049*, China;*
[3]*College of Information Science and Engineering, Jiaxing University, Jiaxing* 314001*, China;*
[4]*School of Information Science and Technology, ShanghaiTech University, Shanghai* 201210*, China;*
[5]*Department of Semiconductor Materials Engineering, Wroclaw University of Science and Technology, Wroclaw* 50-370*, Poland;*
[6]*Department of Microtechnology and Nanoscience, Chalmers University of Technology, Gothenburg* 41296*, Sweden*

Received 14 August 2021/Revised 27 October 2021/Accepted 29 December 2021/Published online 27 June 2022

Abstract Heterogeneous integration of InP and GaSb on Si substrates holds a huge potential interest in near-infrared and mid-infrared optoelectronic devices. In this study, 2-inch 180-nm-thick InP and 185-nm-thick GaSb thin layers were successfully transferred onto the Si substrates to form high-quality and ultra-smooth InP/Si and GaSb/Si templates using molecular beam epitaxy (MBE) and the ion-slicing technique together with selective chemical etching. The relocation of the implantation-introduced damage in the sacrificial layer enables the transfer of relatively defect-free InP and GaSb thin films. The sacrificial layers were completely etched off by selective chemical etching, leaving ultra-smooth epitaxial surfaces with a roughness of 0.2 nm for the InP/Si template and 0.9 nm for the GaSb/Si template, respectively. Thus, the chemical mechanical polishing (CMP) process was not required to smooth the surface which usually introduces particles and chemical contaminations on the transferred templates. Furthermore, the donor substrate is not consumed and can be recycled to reduce the cost, which provides a paradigm for the sustainable and economic development of the Si integration platform.

Keywords heterogeneous integration, InP/Si, GaSb/Si, MBE, ion-slicing technique, selective chemical etching

Citation Jin T T, Lin J J, You T G, et al. Efficient heterogeneous integration of InP/Si and GaSb/Si templates with ultra-smooth surfaces. Sci China Inf Sci, 2022, 65(8): 182402, https://doi.org/10.1007/s11432-021-3398-y

1 Introduction

Heterogeneous integration of III-V compound semiconductor layers with Si substrates has attracted considerable attention since it has great potential applications for combining the III-V-based optoelectronic devices with the Si-based microelectronic circuits [1–6]. Most of the III-V compound semiconductors show substantially higher electron mobility compared with Si [7] and cover a wide spectral window due to the various band gaps [8, 9]. InP-based materials have played a critical role in fiber-optic systems within the 1.1–1.6 μm spectral window, while GaSb-based materials are recognized as the most suitable candidates for high-performance optoelectronics in the 2.0–14 μm mid-infrared range. The heterogeneous integration of InP and GaSb with Si will promote the development of near and mid-infrared optoelectronic integration [10, 11].

* Corresponding author (email: jjlin@mail.sim.ac.cn, shumin@mail.sim.ac.cn, ouxin@mail.sim.ac.cn)
† Jin T T and Lin J J have the same contribution to this work.

© Science China Press and Springer-Verlag GmbH Germany, part of Springer Nature 2022

In order to achieve the heterogeneous integration of InP and GaSb with Si, different methods have been developed, such as heterogeneous epitaxial growth, direct wafer bonding, and ion-slicing technique [7,12–15]. However, the physical constraints between InP, GaSb, and Si, such as the large lattice mismatch (8% for InP/Si and 12% for GaSb/Si), different polarities and large thermal expansion coefficient mismatch (73.1% for InP/Si and 165.4% for GaSb/Si), deleteriously limit the quality of InP and GaSb epitaxial layers directly grown on Si substrates [16–18]. Compared with heterogeneous epitaxial growth, direct wafer bonding can avoid most of these incompatibilities. The ultrathin GaSb template on Si was realized by direct wafer bonding through the Al_2O_3 interlayer and then selectively etched the InAs substrate [19]. Nevertheless, this approach has a relatively high cost since the expensive III-V substrate was completely etched. Alternatively, the ion-slicing technique, as a novel integration route, was used to transfer the III-V layers onto the Si substrates, which combines wafer bonding and undercutting using defect engineering by light ion implantation. Singh et al. [20] successfully transferred the InP layer onto the Si with the surface roughness of ∼8 nm utilizing the spin-on glass (SOG) interlayer via ion-slicing technique. Recently, a wafer-scale no-bubble Si-based InP substrate with lateral outgassing trenches has been obtained by the ion-slicing technique [21]. The donor wafer can be recycled to decrease the cost, but the transferred layer is normally covered by a residual damaged layer with high surface roughness. In order to improve the surface quality, the extra surface treatment process, such as chemical mechanical polishing (CMP) which may increase surface particles and contaminations and cost, is needed after layer transfer to remove the residual damaged layer and reduce the surface roughness [22]. Moreover, the transferred layer tends to suffer from implantation-introduced defects, which is hard to be recovered even by high temperature thermal annealing. Therefore, it remains a challenge to achieve reliable and cost-effective integration for InP and GaSb with Si.

In this study, molecular beam epitaxy (MBE), ion-slicing technique and selective chemical etching have been combined to achieve high-quality wafer-scale Si-based InP and GaSb templates. MBE ensures atomic scale controls of hetero-interfaces between the sacrificial layer and the templates. By adjusting the ion energy, the ion implantation-introduced defects are mainly confined in the sacrificial layers grown by MBE. After the ion-slicing process, selective chemical etching was used to remove the sacrificial layers and exposed the atomically smooth epitaxial surfaces. It can also be used to remove the sacrificial layer on the donor substrate to expose the atomic flat surface for the next MBE growth. This approach not only reduces residual defects in the transferred layer and takes advantage of selective chemical etching to improve the transferred surface conditions without using CMP, but also takes advantage of ion-slicing by remaining the donor substrates for reuse.

2 Experiment

The schematic diagram of our process flow for InP and GaSb layer transfer is shown in Figure 1. The 2-inch (001) InP and GaSb wafers were used as donor substrates to grow InP (200 nm)/$In_{0.53}Ga_{0.47}As$ (800 nm)/InP (200 nm) and GaSb (200 nm)/$InAs_{0.91}Sb_{0.09}$ (600 nm)/GaSb (200 nm) layers by MBE, respectively. In consideration of lattice mismatch and large selective etching ratio with substrates, $In_{0.53}Ga_{0.47}As$ and $InAs_{0.91}Sb_{0.09}$ were selected as sacrificial layers for InP and GaSb [23], respectively. The as-grown heterostructures and the 4-inch (001) Si substrates covered with 500-nm-thick thermal SiO_2 layers were coated with 10-nm-thick Al_2O_3 film by atomic layer deposition (ALD) at 200°C. Al_2O_3 was used as an intermediate layer for the wafer bonding due to its strong hydrophilic nature. For the as-grown InP based heterostructures, H ions were implanted at 95 keV with a fluence of 1×10^{17} cm^{-2} at room temperature. While for the as-grown GaSb based heterostructures, He ions were pre-implanted at 120 keV with a fluence of 2×10^{16} cm^{-2} followed by 5×10^{16} cm^{-2} H ion implantation at 80 keV. The energy of ion implantation was simulated by stopping and range of ions in matter (SRIM) to confine that the implantation-introduced defects mainly existing in the sacrificial layers. After implantation, the as-grown InP and GaSb based heterostructures were directly bonded with Si substrates at room temperature after O_2 plasma activation by using EVG 301 wafer bonder, respectively. Upon subsequent annealing at 250°C for the InP/Si bonding pair and 150°C for the GaSb/Si bonding pair under the N_2 atmosphere, the bonded pairs split at the depth within the sacrificial layers, resulting in the structures of $In_{0.53}Ga_{0.47}As$ (528 nm)/InP (180 nm)/Al_2O_3 (20 nm)/SiO_2 (500 nm)/Si and $InAs_{0.91}Sb_{0.09}$ (451 nm)/GaSb (185 nm)/Al_2O_3 (20 nm)/SiO_2 (500 nm)/Si. The thicknesses of the top InP and GaSb layers designed for the donor substrates are 200 nm, however, the actual growth thicknesses are 180-nm-thick InP

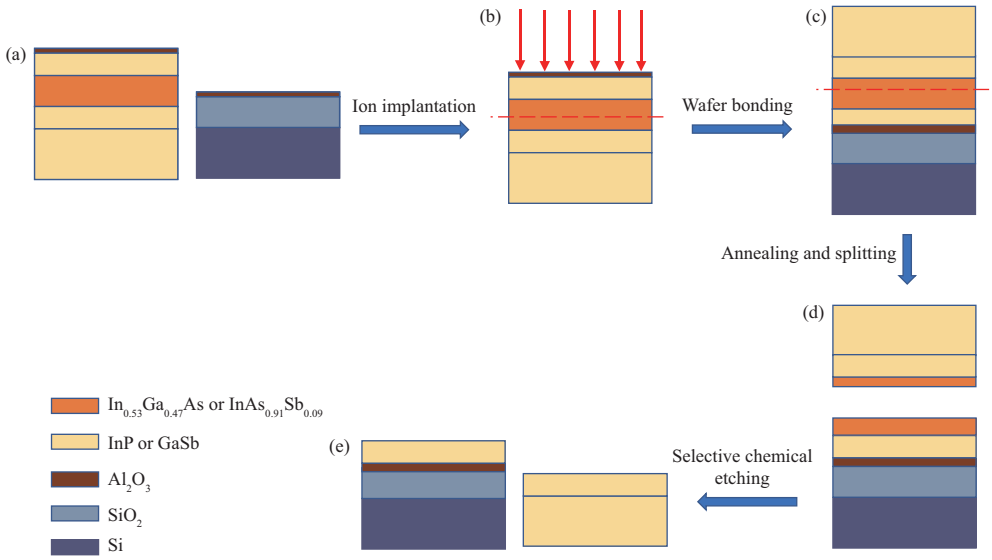

Figure 1 (Color online) Process flow of our scheme for InP and GaSb layers transfer. (a) Heterostructure growth using MBE and Al_2O_3 layers deposition in ALD; (b) He/H ions implantation (dotted line indicates the projected range of the ion implantation); (c) wafer bonding of implanted structures with 4-inch SiO_2/Si substrates; (d) layer splitting after thermal annealing; (e) etching off sacrificial layers by selective chemical etching.

and 185-nm-thick GaSb, respectively, which result from the unstable beam flux and the lack of calibration of the thickness. The top $In_{0.53}Ga_{0.47}As$ layer and $InAs_{0.91}Sb_{0.09}$ layer were etched off by chemical solution H_3PO_4:H_2O_2:H_2O and $C_6H_8O_7$:H_2O_2:H_2O, respectively [24–26]. After the selective chemical etching, the final structures of InP (180 nm)/Al_2O_3 (20 nm)/SiO_2 (500 nm)/Si and GaSb (185 nm)/Al_2O_3 (20 nm)/SiO_2 (500 nm)/Si were obtained. The structures before and after the selective chemical etching were characterized by Raman spectroscopy with HORIBA Scientific LabRAM HR, X-ray diffraction (XRD) with a Philips X'Pert X-ray diffractometer and cross-sectional scanning electron microscopy (SEM) with JEOL 7800F. The analysis of element composition was characterized by energy dispersive spectroscopy (EDS) with JEOL 7800F. The surface topography was characterized by an atomic force microscope (AFM) with Bruker Multimode 8. The quality of the transferred layers was examined by JEOL 2100F filed-emission high-resolution transmission electron microscopy (HRTEM) and selected area electron diffraction (SAED).

3 Results and discussions

The splitting of the as-implanted InP and GaSb heterostructures in the ion-slicing technique requires enough defects introduced by ion implantation in the sacrificial layers. Moreover, sufficient internal pressure in micro-voids is required to fracture III-V bonds and form III-H or V-H bonds. Given that the frictional resistance is constant, the ion penetration depth is a linear function of the implantation energy [27]:

$$d = C_{\mathrm{im}}U, \tag{1}$$

where d is the penetration depth, U is the implantation energy, C_{im} is a constant associated with implantation ions and the material of implanted layer. For the as-implanted InP heterostructure, the parameter C_{im} is fitted as about 7–8 nm/keV, while for the as-implanted GaSb heterostructure, C_{im} is about 3–4 nm/keV [28]. Thus, the implantation energy can be easily estimated for the desired implantation depth. The critical number of implantation ions n_{c} is given by [28]

$$n_{\mathrm{c}} = \frac{8\pi R_0^3 \delta_{\mathrm{c}}}{3kT}\left[1 - \frac{3(1+\nu)\delta_{\mathrm{c}}}{E}\right]^{-1}, \tag{2}$$

where R_0 is the intrinsic void radius, δ_{c} is the fracture stress of the as-implanted layer, k is Boltzmann's constant with a value of 1.38065×10^{-23} J/K, ν is Poisson's ratio and E is Young's modulus. The implantation fluence D is related to the value of n_{c} as follows:

$$D = 2n_{\mathrm{c}}n_{\mathrm{void}}d, \tag{3}$$

Table 1 Main parameters of InAs, GaAs, and InSb [29]

	InAs	GaAs	InSb
a (Å)	6.058	5.65	6.479
ν	0.352	0.31	0.35
E (GPa)	51.4	84.8	409
δ_c (MPa)	2521.46	71.9	100

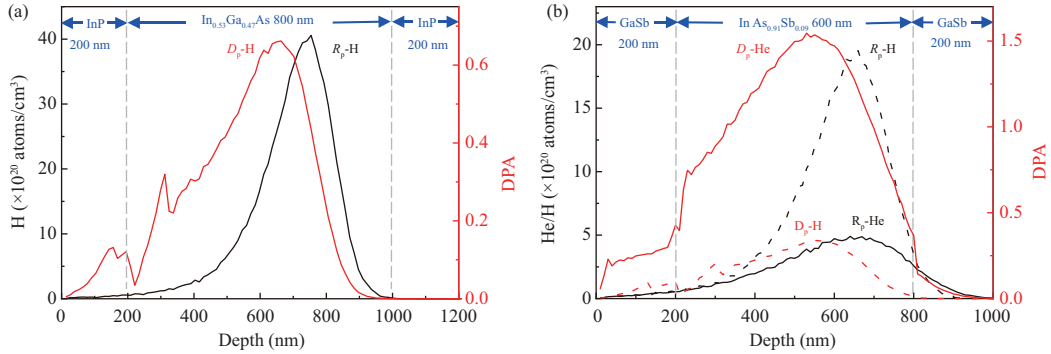

Figure 2 (Color online) Ion distribution and DPA profiles simulated by SRIM in the (a) as-grown InP heterostructure and (b) as-grown GaSb heterostructure.

where n_{void} is the number density of intrinsic voids per unit volume of the as-implanted layer, which can be calculated by

$$n_{\text{void}} = \frac{4}{a^3}, \tag{4}$$

where a is the lattice constant of the as-implanted layer. For the representative parameters of $In_{0.53}Ga_{0.47}As$ and $InAs_{0.91}Sb_{0.09}$ as Table 1 shown, the calculated values of D are 1.85×10^{17} cm^{-2} and 2.875×10^{17} cm^{-2}, respectively. However, in this calculation, the coalescence of defects in thermal annealing is neglected, which leads to getting larger ion fluence than the actual ion fluence for splitting. Hence, based on the simulation, the lower ion fluence was tried in experiments. Ultimately, the precise critical ion fluences were confirmed as 1×10^{17} cm^{-2} H for InP heterostructure splitting and 2×10^{16} cm^{-2} He followed by 5×10^{16} cm^{-2} H for GaSb heterostructure splitting, respectively.

The profiles of the ion distribution and the implantation-introduced damage in terms of displacement per atom (DPA), simulated by SRIM 2008, are shown in Figures 2(a) and (b). The black line indicates the H or He ion distribution, while the red line is the DPA introduced by H or He ion implantation. The peak H concentration (R_p) in the as-grown InP heterostructure locates at depth of ~750 nm and the peak H and He concentration in the as-grown GaSb heterostructure locates at depth of ~670 nm from the surface. Referring to the thickness of each sample (as noted in Figure 2), it is obvious that H and He ions are mainly distributed in the sacrificial layers. The peak distances of DPA, ~660 nm and ~550 nm in the as-grown InP heterostructure and the as-grown GaSb heterostructure, respectively, are smaller than the peak distances of H and He concentration. The implantation-introduced damage is well confined in the sacrificial layers, leaving almost damage-free top InP and GaSb layers.

Following the process flow as shown in Figure 1, a 2-inch wafer-scale InP thin template has been successfully transferred onto a SiO_2/Si substrate. A photo of the InP on the SiO_2/Si substrate is shown in Figure 3(a), in which the InP thin film is highlighted with a white dashed circle. After the layer transfer, selective chemical etching was used to remove the sacrificial layer. To legibly confirm that the $In_{0.53}Ga_{0.47}As$ sacrificial layer was completely etched off, Raman spectra measurement was performed on the transferred layers before and after the selective chemical etching, as shown in Figure 3(b). The (001) Raman spectra were excited by the 514.5 nm laser which can only penetrate to a depth of ~60 nm in the $In_{0.53}Ga_{0.47}As$ layer [30]. Before the selective chemical etching, the weak InAs-like transverse optical (TO) mode at 221 cm^{-1} and the distinct InAs-like longitudinal optical (LO) mode at 229 cm^{-1} appeared, GaAs-like TO mode at 252 cm^{-1} and LO mode at 263 cm^{-1} were also observed in the spectra [31], respectively. After the selective chemical etching, only the LO and TO modes of InP-like appeared instead of the InAs-like and the GaAs-like phonon modes, which indicates that the $In_{0.53}Ga_{0.47}As$ layer was entirely removed. Figure 3(c) shows the XRD rocking curves from the transferred InP (004) plane before and after the

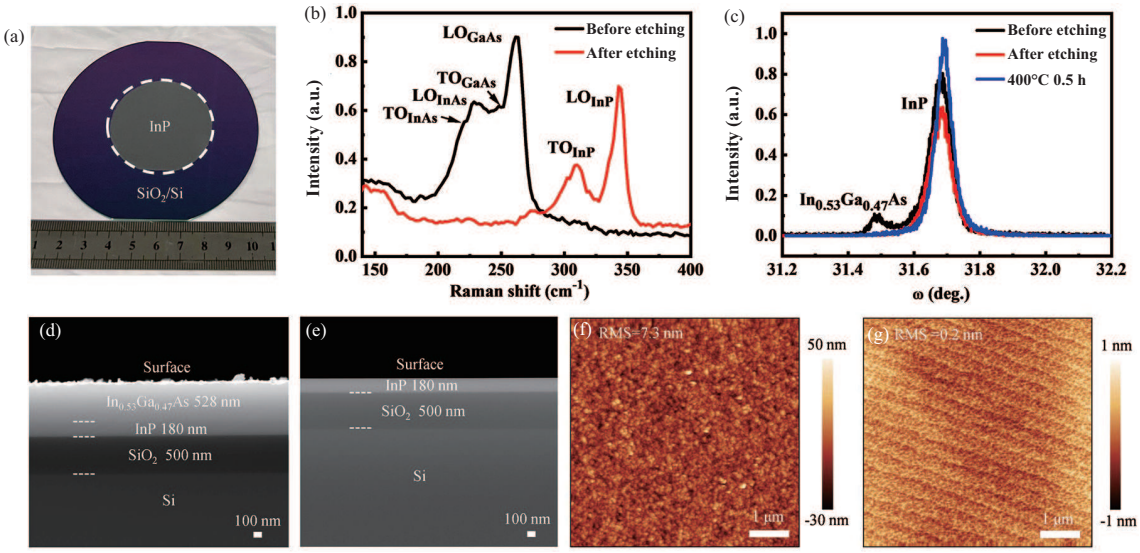

Figure 3 (Color online) (a) The photo image of a 2-inch wafer-scale InP thin template transferred onto a SiO_2/Si substrate. (b) The Raman spectra of the transferred structure before and after the selective chemical etching. (c) The XRD rocking curves from the transferred InP (004) plane before and after the selective chemical etching, together with post-annealing at 400°C. The SEM images of the transferred structure (d) before and (e) after the selective chemical etching. The AFM images of the (f) as-transferred $In_{0.53}Ga_{0.47}As$ surface and (g) InP surface after the selective chemical etching.

selective chemical etching, together with post-annealing at 400°C. Before the selective chemical etching, the peaks of $In_{0.53}Ga_{0.47}As$ and InP were mismatched due to the poorly optimized growth parameters (see Appendix A). The peak of $In_{0.53}Ga_{0.47}As$ disappeared after the selective chemical etching, which indicates that the $In_{0.53}Ga_{0.47}As$ layer has been completely removed, and the full width at half maximum (FWHM) of the remaining InP template was 256 arcsec. After post-annealing at 400°C for 0.5 h, the FWHM was decreased to 208 arcsec, which manifests that annealing at a relatively high temperature can improve the crystalline quality of the InP thin template. SEM was employed to characterize the structure before and after the selective chemical etching, as shown in Figures 3(d) and (e), respectively. Before the selective chemical etching, the distinct hetero-interfaces ($In_{0.53}Ga_{0.47}As$/InP/SiO_2/Si) could be distinguished except for the thin Al_2O_3 layer. The top $In_{0.53}Ga_{0.47}As$ sacrificial layer was ∼528 nm with some particles on the surface, corresponding to layer splitting at the R_p. After the selective chemical etching, the $In_{0.53}Ga_{0.47}As$ layer was removed and the 180-nm-thick InP layer with a smooth surface was exposed. The AFM with a scanning area of 5 μm×5 μm was utilized to evaluate the surface root mean square (RMS) roughness before and after the selective chemical etching, as shown in Figures 3(f) and (g). The as-transferred structure (before the selective chemical etching) had a surface roughness of 7.3 nm, as shown in Figure 3(f). The top $In_{0.53}Ga_{0.47}As$ layer was then completely etched off and the resulting InP surface roughness was 0.2 nm with an obvious atomic step-and-terrace surface, as shown in Figure 3(g), which is sufficiently smooth for the subsequent epitaxial growth. Moreover, the 2-inch donor InP wafer can be recycled after removing the rest $In_{0.53}Ga_{0.47}As$ layer by the selective chemical etching.

With the same process flow, a 2-inch wafer-scale GaSb thin template has been successfully transferred onto a SiO_2/Si substrate without large micro-voids, as marked with a dashed circle in Figure 4(a). Due to the residual particles on the bonding interface, the edge of the template was not transferred. Just as in the case of InP, Raman spectrum was used to examine the changes of composition before and after the selective chemical etching, as shown in Figure 4(b). The 514.5 nm laser used in Raman spectra can only penetrate to a depth of ∼30 nm in $InAs_{0.91}Sb_{0.09}$ layer [30]. The typical TO and LO modes of InAs were found to be 217 and 233 cm^{-1}, respectively [32,33]. The lowest peak at 180 cm^{-1} is the InSb-like interface (IF) mode resulting from Sb incorporation in InAs [31,34], corresponding to the $InAs_{0.91}Sb_{0.09}$ layer of the as-transferred hetero-structure. After the selective chemical etching, the overlapped peaks at 223 and 226 cm^{-1} corresponding to the TO and LO modes of GaSb appeared, respectively, were too close to identify [35,36], which indicates that the $InAs_{0.91}Sb_{0.09}$ sacrificial layer was etched off completely and the GaSb layer was exposed. The crystalline quality of the GaSb template was evaluated by XRD measurements as shown in Figure 4(c). Before the selective chemical etching, the growth parameters of $InAs_{0.91}Sb_{0.09}$ and GaSb were not well optimized causing a small deviation of the observed two peaks.

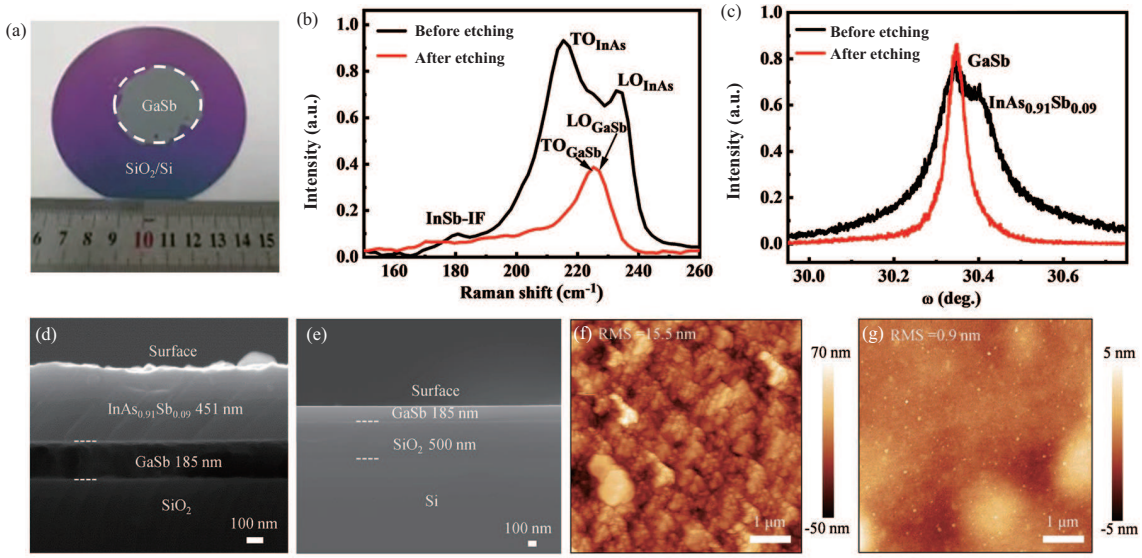

Figure 4 (Color online) (a) The photo image of a 2-inch wafer-scale GaSb thin template transferred onto a SiO_2/Si substrate. (b) The Raman spectra and (c) the XRD rocking curves from the transferred GaSb (004) plane before and after the selective chemical etching. The SEM images of the transferred structure (d) before and (e) after the selective chemical etching. The AFM images of the (f) as-transferred $InAs_{0.91}Sb_{0.09}$ surface and (g) GaSb surface after the selective chemical etching.

After the selective chemical etching, the $InAs_{0.91}Sb_{0.09}$ peak disappeared and the FWHM of the GaSb thin template was 192 arcsec. On the other hand, the structural changes before and after the selective chemical etching were characterized by SEM. For the as-transferred hetero-structure in Figure 4(d), the thickness of the top $InAs_{0.91}Sb_{0.09}$ layer was ∼451 nm, which corresponds to the DPA peak in $InAs_{0.91}Sb_{0.09}$ layer in Figure 2(b). After the selective chemical etching, the sacrificial $InAs_{0.91}Sb_{0.09}$ layer was removed and the 185-nm-thick GaSb layer was exposed, as shown in Figure 4(e). After removing the $InAs_{0.91}Sb_{0.09}$ sacrificial layer, the surface roughness was reduced from 15.5 to 0.9 nm, as shown in Figures 4(f) and (g). Additionally, the donor GaSb wafer can be recycled for next epitaxial growth by etching off the residual $InAs_{0.91}Sb_{0.09}$ layer.

It is noted that there are some particles observed in the AFM image after the selective chemical etching. EDS was used to identify the component of the particles. Figure 5(a) shows the SEM image of one particle (dotted in white line) and the EDS line scanning. Figures 5(b)–(f) show the plane scanning of Ga, Sb, O, Si, and Al elements in the range of the particle, respectively. It is obvious that the Ga and Sb elements aggregate in the particle area, which can be caused by over-etching due to long selective etching time, resulting in GaSb particles produced by uneven speed and anisotropic of the chemical reaction. The optimization of etching time and cleaning process should be further performed to obtain a high-quality surface of the GaSb layer.

The microstructures of the Si-based InP and GaSb were characterized by HRTEM. The cross-sectional TEM (STEM) images of both hetero-structures are shown in the upper regions of Figures 6(a) and (b), respectively. In order to increase the conductivity for a clear HRTEM image, an Au layer was deposited on the surface of the InP layer. The InP layer and the GaSb layer are 180 and 185 nm, respectively, which are consistent with the results of SEM. The Al_2O_3 as the bonding layers in both substrates shows high compactness without any voids, indicating high bonding strength. The crystalline quality of InP and GaSb layers was evaluated by high-angle annular dark field-STEM (HAADF-STEM) and SAED in atomic-scale resolution, as shown in the lower regions of Figures 6(a) and (b), respectively. In HAADF-STEM images, the atoms of InP and GaSb layers are arranged in the regular lattice structure without any visible misfit dislocations. Additionally, SAED images of both layers show regular and bright spots rather than diffraction rings, which suggests that the InP and GaSb layers have a perfect single-crystal structure.

4 Conclusion

In conclusion, the feasibility of InP and GaSb layers transfer using epitaxial growth and the ion-slicing technique together with selective chemical etching has been demonstrated. The implantation-induced

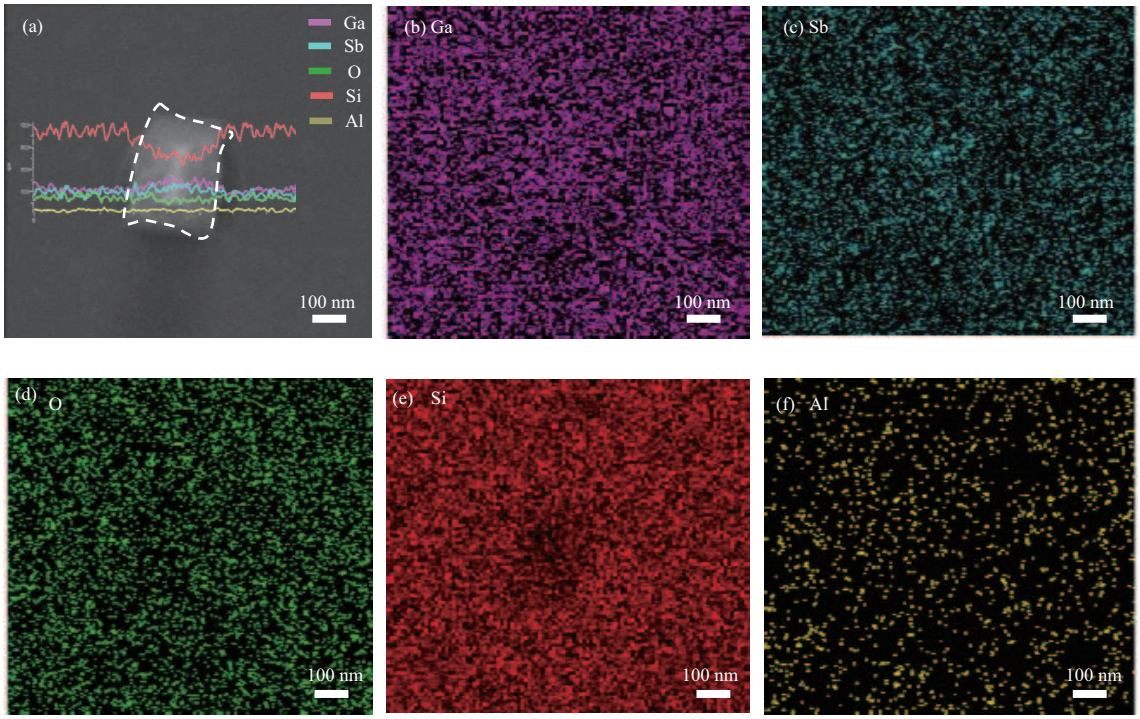

Figure 5 (Color online) (a) The SEM image and the EDS line scanning of the transferred GaSb after the selective chemical etching. (b)–(f) The corresponding EDS surface scanning of elemental Ga, Sb, O, Si, and Al, respectively.

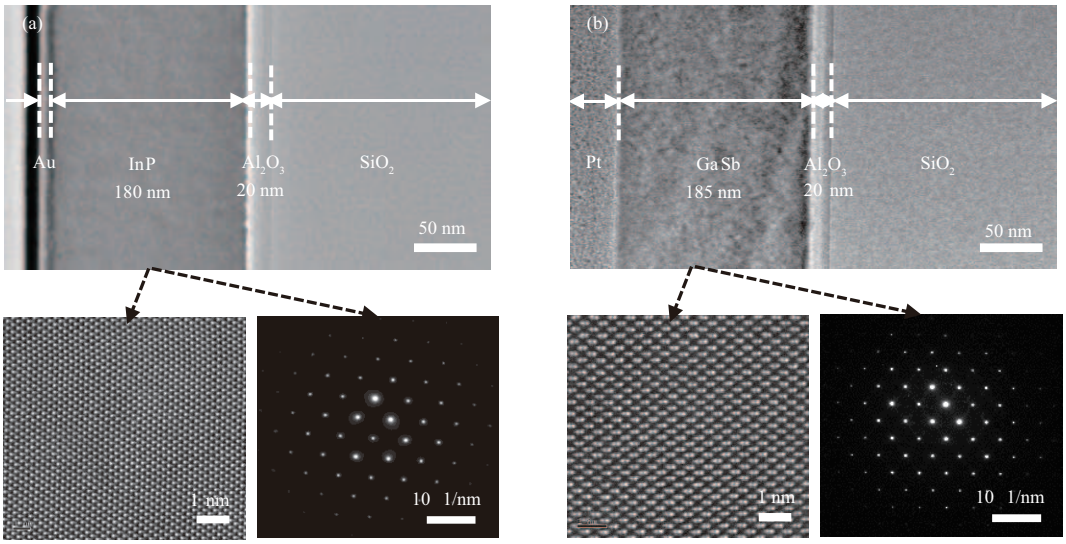

Figure 6 STEM images of the Si-based (a) InP and (b) GaSb templates after the selective chemical etching, in which white dotted lines are interfaces of different materials. The HAADF-STEM images and SAED images of the InP and the GaSb layers are shown below STEM images.

damages were mainly confined in the sacrificial layers to increase the quality of transferred InP and GaSb layers. After layer transfer by ion-slicing, the damaged sacrificial layers were etched off resulting in ultra-smooth surfaces without CMP, 0.2 nm for InP/Si template and 0.9 nm for GaSb/Si template. The monolithic integration of high-quality 2-inch 180-nm-thick InP and 185-nm-thick GaSb templates with 4-inch (001) Si has been successfully fabricated. This technique provides a workable route to fabricate high-quality and ultra-smooth Si-based InP and GaSb heterogeneous templates at a low cost due to the reusable donor substrate.

Acknowledgements This work was supported by National Key RD Program of China (Grant No. 2017YFE0131300), National Natural Science Foundation of China (Grant Nos. U1732268, 61874128, 61851406, 11905282), Frontier Science Key Program of CAS (Grant Nos. QYZDY-SSW-JSC032, ZDBS-LY-JSC009), Program of Shanghai Academic Research Leader (Grant No.

19XD1404600), Shanghai Youth Top Talent Program, Shanghai Sailing Program (Grant Nos. 19YF1456200, 19YF1456400), K. C. Wong Education Foundation (Grant No. GJTD-2019-11), and NCBiR within the Polish-China (Grant No. WPC/130/NIR-Si/2018).

References

1 Keyvaninia S, Verstuyft S, van Landschoot L, et al. Heterogeneously integrated III-V/silicon distributed feedback lasers. Opt Lett, 2013, 38: 5434–5437
2 Hao Y, Xiang S Y, Han G Q, et al. Recent progress of integrated circuits and optoelectronic chips. Sci China Inf Sci, 2021, 64: 201401
3 Fujii T, Takeda K, Nishi H, et al. Multiwavelength membrane laser array using selective area growth on directly bonded InP on SiO_2/Si. Optica, 2020, 7: 838
4 Carter A D, Urteaga M E, Griffith Z M, et al. Q-band InP/CMOS receiver and transmitter beamformer channels fabricated by 3D heterogeneous integration. In: Proceedings of IEEE MTT-S International Microwave Symposium, 2017. 1760–1763
5 Jonsson A, Svensson J, Wernersson L E. A self-aligned gate-last process applied to all-III-V CMOS on Si. IEEE Electron Device Lett, 2018, 39: 935–938
6 Wang R J, Vasiliev A, Muneeb M, et al. III-V-on-silicon photonic integrated circuits for spectroscopic sensing in the 2-4 μm wavelength range. Sensors, 2017, 17: 1788
7 Moutanabbir O, Gösele U. Heterogeneous integration of compound semiconductors. Annu Rev Mater Res, 2010, 40: 469–500
8 Phelan R, Byrne D, O'Carroll J, et al. Mid-infrared inp-based discrete mode laser diodes. In: Optoelectronic Devices. Cambridge: Cambridge University Press, 2019
9 Turner W J, Reese W E, Pettit G D. Exciton absorption and emission in InP. Phys Rev, 1964, 136: 1467–1470
10 Doerr C R. Silicon photonic integration in telecommunications. Front Phys, 2015, 3: 37
11 Guan H, Novack A, Galfsky T, et al. Widely-tunable, narrow-linewidth III-V/silicon hybrid external-cavity laser for coherent communication. Opt Express, 2018, 26: 7920–7933
12 Higurashi E. Heterogeneous integration based on low-temperature bonding for advanced optoelectronic devices. Jpn J Appl Phys, 2018, 57: 04FA02
13 Hjort K. Transfer of InP epilayers by wafer bonding. J Cryst Growth, 2004, 268: 346–358
14 Tong Q Y, Chao Y L, Huang L J, et al. Low temperature InP layer transfer. Electron Lett, 1999, 35: 341
15 Christiansen S H, Singh R, Gosele U. Wafer direct bonding: from advanced substrate engineering to future applications in micro/nanoelectronics. Proc IEEE, 2006, 94: 2060–2106
16 Levinshtein M, Rumyantsev S, Shur M. Handbook Series on Semiconductor Parameters. Singapor: World Scientific, 1996
17 Akahane K, Yamamoto N, Gozu S, et al. Heteroepitaxial growth of GaSb on Si(001) substrates. J Cryst Growth, 2004, 264: 21–25
18 Arpapay B, Suyolcu Y E, Çorapçıoğlu G, et al. A comparative study on GaSb epilayers grown on nominal and vicinal Si(100) substrates by molecular beam epitaxy. Semicond Sci Technol, 2020, 36: 025011
19 Yokoyama M, Yokoyama H, Takenaka M, et al. Ultrathin body GaSb-on-insulator p-channel metal-oxide-semiconductor field-effect transistors on Si fabricated by direct wafer bonding. Appl Phys Lett, 2015, 106: 073503
20 Singh R, Radu I, Scholz R, et al. Low temperature InP layer transfer onto Si by helium implantation and direct wafer bonding. Semicond Sci Technol, 2006, 21: 1311–1314
21 Lin J J, You T G, Wang M, et al. Efficient ion-slicing of InP thin film for Si-based hetero-integration. Nanotechnology, 2018, 29: 504002
22 Mazen F, Sollier S, Madeira F, et al. Fracture in epitaxial InP on Si for InGaAs on insulator fabrication via smart cut^{TM}. In: Proceedings of the 21st International Conference on Ion Implantation Technology (IIT), 2016. 1–4
23 Clawson A R. Guide to references on III-V semiconductor chemical etching. Mater Sci Eng-R-Rep, 2001, 31: 1–438
24 Hjort K. Sacrificial etching of III-V compounds for micromechanical devices. J Micromech Microeng, 1996, 6: 370–375
25 Dier O, Lin C, Grau M, et al. Selective and non-selective wet-chemical etchants for GaSb-based materials. Semicond Sci Technol, 2004, 19: 1250–1253
26 Grzesik M, Vangala S R, Goodhue W D. Indirect wafer bonding and epitaxial transfer of GaSb-based materials. J Elec Materi, 2013, 42: 679–683
27 Bruel M. Application of hydrogen ion beams to silicon on insulator material technology. Nucl Instrum Method Phys Res Sect B-Beam Interact Mater Atoms, 1996, 108: 313–319
28 Feng X Q, Huang Y. Mechanics of smart-cut(r) technology. Int J Solids Struct, 2004, 41: 4299–4320
29 Martienssen W. Springer Handbook of Condensed Matter and Materials Data. Berlin: Springer, 2005
30 Aspnes D E, Studna A A. Dielectric functions and optical parameters of Si, Ge, GaP, GaAs, GaSb, InP, InAs, and InSb from 1.5 to 6.0 eV. Phys Rev B, 1983, 27: 985–1009
31 Georgiev N, Mozume T. Raman scattering analysis of InGaAs/AlAsSb short-period superlattices. Appl Surf Sci, 2000, 159: 520–527
32 Chen L C, Tyan S L, Wu M C. Raman scattering of $InAs_{1-x-y}Sb_xP_y$ quaternary alloys. Jpn J Appl Phys, 1998, 37: 1365–1366
33 Cai L C, Chen H, Bao C L, et al. Raman spectroscopic studies of InAs epilayers grown on the GaAs (001) substrates. J Cryst

Growth, 2003, 253: 112–116

34 Xu D P, Litvinchuk A P, Wang X, et al. Structure stability of short-period InAs/AlSb superlattices. J Cryst Growth, 2003, 251: 547–550

35 Milekhin A, Werninghaus T, Zahn D R T, et al. Raman and infrared spectroscopical investigation of the optical vibrational modes in GaSb/AlSb superlattices. Eur Phys J B, 1998, 6: 295–299

36 Qiao Z X, Yun S, He W Y, et al. Raman scattering of polycrystalline GaSb thin films grown by the co-evaporation process. Chin Phys B, 2009, 18: 2012–2015

Appendix A

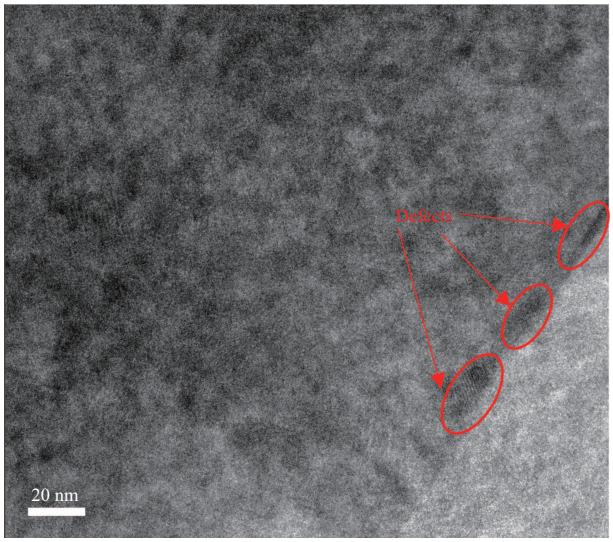

Figure A1 (Color online) STEM image of the $In_{0.53}Ga_{0.47}As$/InP interface before selective chemical etching.

There are two main influencing factors about the quality of layers, epitaxial growth and ion implantation, respectively. However, it has been confirmed that the ion implantation process will only broaden the full width at half maximum (FWHM) of the InP template, and has no influence on the shift of peak position. Figure A1 shows the STEM image of the $In_{0.53}Ga_{0.47}As$/InP interface before the selective chemical etching. It is obvious that there are some defects along with the interface, which indicates the mismatch of $In_{0.53}Ga_{0.47}As$ and InP during epitaxial growth. Therefore, it is reasonable that the mismatched peaks of $In_{0.53}Ga_{0.47}As$ and InP result from the poorly optimized growth parameters of epitaxial growth.